Rotationally resolved laser-induced fluorescence of biacetyl in A 1Au–X1Ag

Cheng-Liang Huang, Hon-Huei Liu, Chen-Lin Liu, A. H. Kung, and Chi-Kung Ni

Citation: J. Chem. Phys. **117**, 5165 (2002); doi: 10.1063/1.1499489
View online: http://dx.doi.org/10.1063/1.1499489
View Table of Contents: http://jcp.aip.org/resource/1/JCPSA6/v117/i11
Published by the American Institute of Physics.

Rotationally resolved laser-induced fluorescence of biacetyl in $A\,^1A_u - X\,^1A_g$

Cheng-Liang Huang, Hon-Huei Liu, Chen-Lin Liu, A. H. Kung, and Chi-Kung Ni[a)]
Institute of Atomic and Molecular Sciences, Academia Sinica, Taipei, 106, P.O. Box 23-166 Taiwan

(Received 6 May 2002; accepted 19 June 2002)

Laser-induced fluorescence of jet-cooled biacetyl was recorded in the region of 22 177–22 277 cm^{-1} with a resolution of 0.012 cm^{-1}. Three bands, 0_0^0, 15_0^1, and 21_0^1 with transitions $J'' \leqslant 3$ were observed and analyzed. For the 0_0^0 band, E_2-E_1 and $G-G$ subbands were observed. However, only *c*-type transitions, $\Delta K_a = \text{odd}$, $\Delta K_c = \text{even}$, were observed. Another kind of transition, *d*-type ($\Delta K_a = \text{even}$, $\Delta K_c = \text{even}$), which is allowed by selection rules, was not observed. For the 15_0^1 band, two subbands E_3-E_3 and $G-G$ were observed. The E_3-E_3 subband can be described by the rigid rotor model, and it contains only $\Delta K_a = \text{odd}$, $\Delta K_c = \text{even}$ transitions. On the other hand, the $G-G$ subband cannot be even approximately described by the rigid rotor model. It is dominated by *c*-type transitions. In addition, *a*/*b*-type and *d*-type transitions were all observed, though the intensities are small. For the 21_0^1 band, E_2-E_1, $G-G$, and A_3-A_1 subbands were observed. The E_2-E_1, $G-G$ subbands contain all the possible types of transitions, i.e., *a*/*b*-and *c*/*d*-type transitions. However, the A_3-A_1 subband has $\Delta K_a = \text{odd}$, $\Delta K_c = \text{even}$ transitions only. The band origin, rotational constants, and the splitting due to the tunneling in these three bands was accurately measured. Relatively large vibronic transition intensities were observed in both the 15_0^1 and 21_0^1 bands. © *2002 American Institute of Physics.* [DOI: 10.1063/1.1499489]

I. INTRODUCTION

Biacetyl is the first molecule in which fluorescence quantum beat modulation was observed.[1,2] Most of the transitions of biacetyl between the electronic ground state $X\,^1A_g$ and the first singlet excited state $A\,^1A_u$ show quantum beat intensity modulation in fluorescence decay due to the strong interaction between the singlet and triplet states. Though the spectroscopy has been studied intensively since two decades ago,[1–10] many questions still remain, mainly because the relatively large number of atoms and the high density of states in biacetyl makes the spectrum congested. The two internally rotating methyl groups in biacetyl also make the spectroscopic analysis not straightforward.

Biacetyl exhibits an absorption spectrum in the 520–350 nm region, which has a broad structureless appearance at room temperature. The first analysis of the vibronic structure was carried out by Sidman and McClure,[3] who studied the spectrum in the solid phase at 4 K. They concluded that the principal transitions belong to the π^*-n electronic transitions $A\,^1A_u - X\,^1A_g$ and $a\,^3A_u - X\,^1A_g$. The experiment of van der Werf and Kommandeur[4] showed that the zero-pressure luminescence is composed of a fast fluorescence and a slow phosphorescence, and the luminescence was attributed to the decay of a mixed state with both singlet ($A\,^1A_u$) and triplet ($a\,^3A_u$) character. Jet-cooled laser-induced fluorescence excitation spectra, LIF, of $A\,^1A_u(S^1) - X\,^1A_g(S^0)$ were studied extensively by Campargue and Soep,[5] and Chaiken *et al.*[1,2] Their cold spectra showed a remarkable simplification with respect to the room temperature spectra. The lowest-energy band that was observed in the cold jet spectrum at 22 336 cm^{-1} was assigned to be the band origin of the $A\,^1A_u - X\,^1A_g$ transition. However, Herschbach *et al.*[6] observed three bands to the red of 22 336 cm^{-1} under warm and cold jet conditions, and reassigned the band origin at 22 182 cm^{-1}. Senent *et al.* carried out theoretical simulations of the cold jet fluorescence excitation spectrum and also placed the band origin at 22 182 cm^{-1}.[7] The theoretical simulation predicted the tunneling splitting in the first and second vibrational bands to be 1.1 and 1.7 cm^{-1}, respectively. Recently, cold jet fluorescence spectra at a resolution of 0.07 cm^{-1} were obtained for the first and second vibrational bands by Chen *et al.*,[8] who observed only two prominent peaks in each vibrational band. They suggested that these two peaks correspond to the tunneling splitting predicted by the theoretical simulation rather than to rotational structure, and thus also assigned the band origin at 22 182 cm^{-1}.

In contrast to the vibronic spectrum of biacetyl, the rotationally resolved spectrum has received little attention. Gurnick *et al.*[2] obtained rotationally resolved LIF spectra of the 0–0 and 160 cm^{-1} bands of the $A\,^1A_u - X\,^1A_g$ transition between 22 336 and 22 496 cm^{-1} in a molecular beam. (Based on the present work, the new assignments for these two bands are the 154 and 314 cm^{-1} bands.) The analysis of Gurnick *et al.*[2] yields rotational constants for biacetyl of $A = 0.24$, $B = 0.16$, and $C = 0.09$ cm^{-1} in both the $X\,^1A_g$ and $A\,^1A_u$ states. Henke *et al.*[9] studied the partially rotationally resolved spectra of the 280 cm^{-1} band (the new assignment is the 434 cm^{-1} band). However, they found that rotational constants of $A = 0.176$, $B = 0.105$, $C = 0.0675$ cm^{-1} in both the $X\,^1A_g$ and $A\,^1A_u$ states, as obtained from the known covalent radii and 120° band angles, gave much better agreement with the experimental spectra. Note that the rotational constants obtained in Refs. 2 and 10 differ by about 30%.

a)Author to whom correspondence should be addressed. Electronic mail: ckni@po.iams.sinica.edu.tw

In this work, we recorded the jet-cooled laser-induced fluorescence spectrum of biacetyl in the energy region from 22 177 to 22 277 cm^{-1} with a resolution of 0.012 cm^{-1}. The rotationally resolved structure of three vibrational bands, 0_0^0, 15_0^1, and 21_0^1, and various associated tunneling splittings were observed and analyzed.

II. EXPERIMENT

A cw ring Ti:Al_2O_3 laser (Coherent 899/29) pumped with an Ar^+ laser served to generate the seeding beam. An amplifier chain containing one dye preamplifier and one Ti:Al_2O_3 power amplifier pumped with a Nd:YAG laser was used to amplify this seeding beam to yield pulses at energies of 20 mJ/pulse and a repetition rate of 30 Hz. This laser system has been described in detail elsewhere.[10,11] The output of the amplifier was mixed with a 1064 nm laser beam from an injection seeded Nd:YAG laser in a BBO crystal to generate pulses at about 445–450 nm. After frequency mixing, the UV beam had an energy of 1–2 mJ/pulse with a 2 ns pulse duration and a bandwidth of ~140 MHz.

Biacetyl seeded in helium (0.06%) in a supersonic jet was detected through laser-induced fluorescence spectra via the transition $A\,^1A_u - X\,^1A_g$. Gaseous mixtures were expanded through an orifice (General Valve, diameter 0.8 mm) into a vacuum chamber with a stagnation pressure of 3 or 9 atm. The laser beam intersected the molecular jet 30 mm downstream from the outlet of the pulsed valve; near the intersection region the diameter of the laser beam was 3 mm. The total emission of biacetyl was collected through a spatial filter to decrease the spectral full width at half-maximum to 0.012 cm^{-1}. A long pass filter (Corion OG515) and a short pass filter (Andover 700FL07-50S) in combination with baffles in both arms of the vacuum chamber served to eliminate scattered light. The spectra were recorded with a photon counter and averaged over 100 laser shots at each point with a step size of 50 MHz. The absolute wavelength was calibrated with Ne optogalvanic spectroscopy. The precision of relative positions in the combined spectra is expected to be within 0.004 cm^{-1}. Fluorescence decays of individual levels were recorded with a multichannel scaler and accumulated for 2×10^4 laser shots. The dwell of the multichannel scaler was set at 5 ns, and the total record length was 81 μs.

III. SYMMETRY SPECIES AND SELECTION RULES

We divide our discussion of symmetry species and selection rules into two parts. The first part is based on traditional point group ideas,[12] since these are more familiar and easier to understand. Strictly speaking, however, these point group ideas are applicable to biacetyl only if the two methyl groups do not internally rotate, i.e., do not give rise to observable torsional tunneling splittings. The second part is based on permutation-inversion group ideas,[13,14] and describes the changes in symmetry labels and selection rules that are required by the fact that internal rotation of the two methyl groups does, in fact, give rise to easily observable splittings in the biacetyl spectrum.

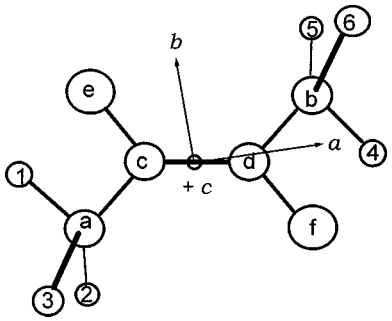

FIG. 1. Geometric structure of biacetyl in the ground electronic state. For the geometric structure in the electronic excited state, both of the methyl groups rotate 60°.

A. C_{2h} point group treatment

In the ground electronic state, $X\,^1A_g$, the two methyl groups of biacetyl are attached to the planar α-carbonyl framework in a *trans* configuration. The equilibrium geometric structure obtained from an *ab initio* calculation, as shown in Fig. 1, belongs to the point group C_{2h}. In the electronic excited state, $A\,^1A_u$, the α-carbonyl framework remains planar, but both methyl groups undergo a 60° rotation. This rotation of the methyl groups in the excited state results in a long progression in the methyl torsion. The equilibrium structure in the excited state, $A\,^1A_u$, also belongs to the point group C_{2h}. The symmetry species for the ground electronic state and the electronic excited state are A_g and A_u, respectively. The vibrational states under study in this work are the ground state (A_g), the first gearing mode $\nu_{15}=1(A_u)$, and the first antigearing mode $\nu_{21}=1(B_g)$. Symmetry species for rotational levels are A_g for even quantum number K_c, and B_g for odd quantum number K_c. The intensity of the $A\,^1A_u - X\,^1A_g$ transitions can be calculated from the equation

$$I = P_i g_i |\langle \psi_i | \mu_Z | \psi_f \rangle|^2, \tag{1}$$

where P_i is the population, g_i is the nuclear spin weight, ψ_i and ψ_f are the initial and final state wave functions, and μ_Z is the electric transition dipole in the laboratory frame. Equation (1) can be further approximated by the following expressions:

$$I = P_i g_i |\langle \Psi_{ievr} | \mu_Z | \psi_{fevr} \rangle|^2 \tag{2}$$

$$\begin{aligned} &\cong P_i g_i \{ |\langle \psi_{iev} | \mu_x | \psi_{fev} \rangle|^2 \times |\langle \psi_{ir} | \Phi_{Zx} | \psi_{fr} \rangle|^2 \\ &\quad + |\langle \psi_{iev} | \mu_y | \psi_{fev} \rangle|^2 \times |\langle \psi_{ir} | \Phi_{Zy} | \psi_{fr} \rangle|^2 \\ &\quad + |\langle \psi_{iev} | \mu_z | \psi_{fev} \rangle|^2 \times |\langle \psi_{ir} | \Phi_{Zz} | \psi_{fr} \rangle^2 \}, \end{aligned} \tag{3}$$

$$\begin{aligned} &\cong P_i g_i \{ |\langle \psi_{ie} | \mu_{0x} | \psi_{fe} \rangle|^2 \times |\langle \psi_{iv} | \psi_{fv} \rangle|^2 \times |\langle \psi_{ir} | \Phi_{Zx} | \psi_{fr} \rangle|^2 \\ &\quad + |\langle \psi_{ie} | \mu_{0y} | \psi_{fe} \rangle|^2 \times |\langle \psi_{iv} | \psi_{fv} \rangle|^2 \times |\langle \psi_{ir} | \Phi_{Zy} | \psi_{fr} \rangle|^2 \\ &\quad + |\langle \psi_{ie} | \mu_{0z} | \psi_{fe} \rangle|^2 \times |\langle \psi_{iv} | \psi_{fv} \rangle|^2 \times |\langle \psi_{ir} | \Phi_{Zz} | \psi_{fr} \rangle|^2 \}, \end{aligned} \tag{4}$$

where μ_x, μ_y, and, μ_z are the electric dipole operator components in the molecular frame, and Φ are direction cosine matrix elements. In Eq. (4), the dipole moment components μ_i $(i=x,y,z)$ are further approximated by μ_{0i}, where the nuclear coordinate dependence of both the dipole moment operator and the electronic wave function is neglected.

TABLE I. Character table for G_{36}.

	E	$(123)(456)$	$(14)(26)(35)(ab)(cd)(ef)^*$	$(123)(465)$	(132)	$(142635)(ab)(cd)(ef)^*$	$(14)(25)(36)(ab)(cd)(ef)$	$(142536)(ab)(cd)(ef)$	$(23)(56)^*$	
Operation	1	2	3	2	4	6	3	6	9	
Equiv. rot.	R_0	R_0	R_0	R_0	R_0	R_0	R_c^π	R_c^π	R_c^π	
A_1	1	1	1	1	1	1	1	1	1	α_{zc}
A_2	1	1	1	1	1	1	−1	−1	−1	α_{za}, α_{zb}
A_3	1	1	−1	1	1	−1	1	1	−1	T_c
A_4	1	1	−1	1	1	−1	−1	−1	1	T_a, T_b
E_1	2	2	2	−1	−1	−1	0	0	0	
E_2	2	2	−2	−1	−1	1	0	0	0	
E_3	2	−1	0	2	−1	0	2	−1	0	
E_4	2	−1	0	2	−1	0	−2	1	0	
G	4	−2	0	−2	1	0	0	0	0	

Equation (2) gives the most rigorous selection rules, but they only apply to overall rovibronic (evr) symmetry species. These selection rules may be summarized as ${}^{evr}A_g \leftrightarrow {}^{evr}A_u$ and ${}^{evr}B_g \leftrightarrow {}^{evr}B_u$. Equations (3) and (4) give more restrictive, but more approximate, selection rules. Thus, the K_c selection rule derived from Eq. (3) is $\Delta K_c = \text{even}$ for the 0_0^0 band, the 15_0^1 band transition is not allowed by Eq. (3), and the K_c selection rule for the 21_0^1 band is $\Delta K_c = odd$. We also find that the third term in Eq. (3) is the only nonzero term for the 0_0^0 band, which results from a vibronic transition dipole moment along the c axis. On the other hand, the first and the second terms in Eq. (3) are the nonzero terms in the 21_0^1 band, which results from vibronic transition dipole moments along the a and b axes. Since the $A\,{}^1A_u - X\,{}^1A_g$ transition is orbitally an ${}^eA_u - {}^eA_g$ transition, Eq. (4) shows that only the third term (transition dipole moment along the c axis) is electronically allowed. Therefore, transitions with $\Delta K_c = even$ are expected to have larger intensities than transitions with $\Delta K_c = odd$. As a result, the vibronic transitions in biacetyl can be divided into two types, which we call *ab*-type and *cd*-type in this paper. Transitions of the *ab*-type follow traditional rigid-rotor *ab*-hybrid selection rules, i.e., $\Delta K_c = odd$ and $\Delta K_a = even$ or *odd*. Transitions of the *cd*-type follow the selection rule, $\Delta K_c = even$. In other words, transitions of *c*-type follow rigid-rotor *c*-type selection rules, i.e., $\Delta K_c = even$, $\Delta K_a = odd$, and transitions that we call *d*-type here are forbidden in the rigid-rotor approximation, i.e., $\Delta K_c = even$, $\Delta K_a = even$.

B. G_{36} permutation–inversion symmetry group treatment

When internal rotation is considered, both electronic states, $X\,{}^1A_g$ and $A\,{}^1A_u$, are described by the molecular symmetry group G_{36}. In this case, each level of the rigid C_{2h} model splits into four sublevels, one nondegenerate A_i state, two doubly degenerate E_i states, and one fourfold degenerate G state for a total degeneracy of nine. The magnitude of the splitting of the levels depends on the degree of restriction of the internal rotational motion of the two methyl groups. At the bottom of the well the torsional splitting of the levels may be very small, whereas at the top of the well the levels are widely separated. The character table of the G_{36} group is shown in Table I.[15]

Quantitative examples of this splitting for biacetyl are given in Table IV of Ref. 7, where *ab initio* potential surfaces and a G_{36} symmetry-adapted Hamiltonian were used to calculate wave numbers for various allowed transitions from the ground vibronic state to vibronic states of the first excited singlet and first excited triplet electronic states containing from zero to two vibrational quanta in the geared and/or antigeared torsional modes.

The overall selection rules obtained from Eq. (2) in G_{36} are ${}^{evr}A_1 \leftrightarrow {}^{evr}A_3$, ${}^{evr}A_2 \leftrightarrow {}^{evr}A_4$, ${}^{evr}E_1 \leftrightarrow {}^{evr}E_2$, ${}^{evr}E_3 \leftrightarrow {}^{evr}E_3$, ${}^{evr}E_4 \leftrightarrow {}^{evr}E_4$, and ${}^{evr}G \leftrightarrow {}^{evr}G$. The application of permutation–inversion group ideas to the analog of Eq. (4) requires a rather complete analysis of the coordinate system used to factor the rovibronic function into electronic, vibrational, and rotational components, primarily because the introduction of one or more large-amplitude coordinates, the introduction of different equilibrium frameworks, and the locking of the rotational axes to the floppy molecule (i.e., the definition of the rotational angles) can be carried out in a large variety of ways. Each way can, in turn, lead to a different definition for the electronic, large-amplitude-vibrational, small-amplitude-vibrational, and rotational basis functions, and therefore to a different set of selection rules on the quantum numbers for these basis functions. Since a complete analysis of the coordinate system will not be carried out in this paper, a complete set of G_{36} selection rules will not be derived from Eq. (4).

It is possible, however, to make the following intuitive arguments concerning the use of Eq. (3). Because the internal rotation motion of one or both of the methyl groups does not (to a very good approximation) change the moments of inertia of biacetyl, it is reasonable to imagine keeping the rotational axes locked to the planar α-carbonyl framework for any G_{36} treatment, just as they were for the C_{2h} treatment in the previous section. Because the observed tunneling splittings are not large, the $G_{36}K_{cp}$, K_c values of observed levels can be determined from the K_{cp}, K_c values of their C_{2h} parent level, and the G_{36} symmetry species of the K_{cp}, K_c rotational functions can be obtained from their C_{2h} symmetry species and a correlation table. In particular, symmetry species for rotational basis functions are A_1 for even values of the quantum number K_c, and A_2 for odd values of K_c.

If one uses the ideas above to construct rotational energy level diagrams for each G_{36} vibronic symmetry species, one

TABLE II. Selection rules, rotational constants and band origins.

	Selection rules[a]	Exp.	Origin exp.	Origin cal.[b]	A'	B'	C'	A''	B''	C''
0_0^0 $G-G$	*a, b, c, d*	*c*	22 178.498	22 178.498	0.1758	0.1135	0.0700	0.1768	0.1128	0.0710
0_0^0 E_2-E_1	*a, b, c, d*	*c*	22 178.576	22 178.608	0.1745	0.1134	0.0710	0.1763	0.1130	0.0710
15_0^1 E_3-E_3	*c, d*	*c*	22 264.951	22 264.318	0.1759	0.1142	0.0710	0.1772	0.1119	0.0720
15_0^1 $G-G$	*a, b, c, d*	*a, b, c, d*	22 265.964	22 265.458						
21_0^1 E_2-E_1	*a, b, c, d*	*a, b, c, d*	22 274.691	22 273.698						
21_0^1 $G-G$	*a, b, c, d*	*a, b, c*	22 276.304	22 275.458						
21_0^1 A_3-A_1	*a, b*	*a*	22 277.554	22 276.738	0.1950	0.1110	0.0697	0.1970	0.1142	0.0703

[a]From the G_{36} symmetry group.
[b]From Ref. 8. The calculated value of 0_0^0 $G-G$ transition has been adjusted to match the experimental value. Unit: cm^{-1}.

finds that the selection rules are very similar to that derived from C_{2h} point group. Vibronic transitions in biacetyl can be divided into two types, i.e., transitions of *ab*-type follow the selection rule $\Delta K_c = odd$ and transitions of *cd*-type follow the selection rule $\Delta K_c = even$.

For the 0_0^0 band, selection rules obtained from Eq. (3) in the G_{36} molecular symmetry group show that there are four subbands allowed. Both the E_2-E_1 and G–G subbands have *ab*- and *cd*-type rotational transitions; whereas A_3-A_1 and E_3-E_3 subbands have only *cd*-type transitions. For the 15_0^1 band, only two subbands are allowed. The E_3-E_3 subband has *cd*-type transitions, and the G–G subband has *ab*- and *cd*-type transitions. There are four subbands allowed in the 21_0^1 band according to the selection rules. Both E_2-E_1 and G–G subbands have *ab*- and *cd*-type transitions, whereas A_3-A_1 and E_3-E_3 only have *ab*-type transitions. The selection rules obtained from G_{36} are summarized in Table II.

IV. RESULTS AND DISCUSSION

A. 0_0^0 band

LIF spectra of the biacetyl 0_0^0 band were obtained at two stagnation pressures, 3 and 9 atm, which gave slightly different rotational temperatures. For 9 atm, only $J=0$, 1, and 2 levels are populated, and the spectra were best described by a rotational temperature of 0.5 K. On the other hand, $J=3$, and 4 levels are also populated at a stagnation pressure of 3 atm; this spectrum is shown in Fig. 2.

For the 0_0^0 band, there are four subbands allowed according to the selection rules from the G_{36} group. However, only two subbands were observed. One has intensity about five times larger than the other. We assigned the large-intensity, low-transition frequency subband to a G–G transition and the small-intensity, high-transition frequency subband to an E_2-E_1 transition, based on the statistical weights (nuclear spin and vibrational degeneracy) and the theoretically predicted[5] transition frequencies. The rotational selection rule for these two subbands is $\Delta K_c = even$, i.e, there are two kinds of transitions: $\Delta K_a = odd$, $\Delta K_c = even$ and $\Delta K_a = even$, $\Delta K_c = even$. However, only the *c*-type transitions with $\Delta K_a = odd$, $\Delta K_c = even$ were observed. For the total of 58 lines we observed in this band, 54 lines were assigned. Only transition frequencies at 22 178.286, 22 178.391, 22 178.713, and 22 179.168 cm^{-1} remain unassigned. The fluorescence decay rates of these lines are about the same as the other lines, and they also show quantum beat intensity modulation. Therefore, they must result from molecules of biacetyl. It is possible that these lines belong to one of the A_3-A_1 or E_3-E_3 subbands. Since there are only four lines unassigned, and most of the transitions belonging to A_3-A_1 or E_3-E_3 are obscured by the E_2-E_1 and G–G transitions, no attempt was made to assign these transitions. No observation of A_3-A_1 or E_3-E_3 subbands is likely since the statistical weight results in a low intensity for A_3-A_1 and E_3-E_3 transitions.

All the assigned transition frequencies in the 0_0^0 can be described very well by the rigid asymmetric rotor Hamiltonian. Tables III and IV list transition frequencies and assignments for these two subbands. The rotational constants obtained from a rigid asymmetric rotor fit of the experimental data are listed in Table II. The difference in band origins between the G–G and E_2-E_1 transitions due to the tunneling splitting is 0.078 cm^{-1} from our experimental measurements.

Some of the assignments of the spectrum obtained at 9 atm were further confirmed by their upper state fluorescence quantum beat decay patterns. For example, the essentially identical fluorescence quantum beat decay patterns displayed in Fig. 3 show that the transition assigned as $1_{11} \leftarrow 2_{21}$ and the transition assigned as $1_{11} \leftarrow 1_{01}$ have the same upper state. The quantum beat fluorescence decay patterns are also labeled by arbitrary counters (e.g., W1, W2,...) in Table IV. No attempt was made to obtain quantum beat patterns for the

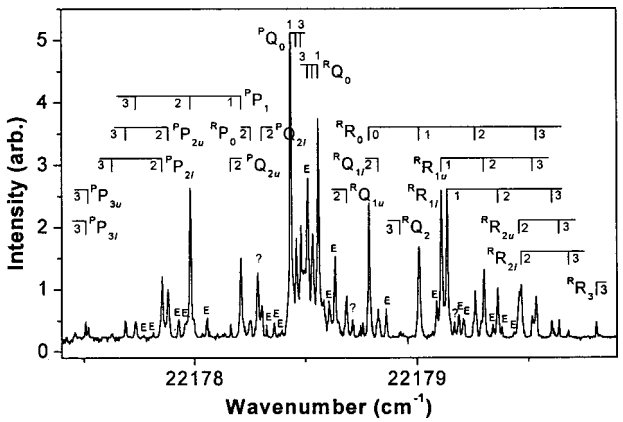

FIG. 2. Part of the spectrum of the 0_0^0 band. The assignments are shown only for $G-G$ transitions and the peaks labeled by E are E_2-E_1 transitions. All of the assignments are $\Delta K_a = odd$, $\Delta K_c = even$ transitions.

TABLE III. Observed 0_0^0 $G-G$ transitions (cm^{-1}).

J'	Ka'	Kc'	J''	Ka''	Kc''	Obs.	Obs–cal.	Q.B.[a]
2	2	1	3	3	1	22 177.5087	−0.001	
2	2	0	3	3	0	22 177.5203	−0.002	
2	1	2	3	2	2	22 177.6271	0.002	
2	1	1	3	2	1	22 177.6854	−0.005	
2	0	2	3	1	2	22 177.7338	0.003	
1	1	1	2	2	1	22 177.8539	0.001	W1
1	1	0	2	2	0	22 177.8806	−0.001	W2
1	0	1	2	1	1	22 177.9823	0.0003	W4
2	1	2	2	2	0	22 178.1641	0.002	
0	0	0	1	1	0	22 178.2108	0.003	
1	1	0	2	0	2	22 178.2542	0.003	
2	1	1	2	2	1	22 178.3042	−0.003	
3	1	2	3	2	2	22 178.3576	−0.0004	
1	0	1	1	1	1	22 178.4319	−0.002	W4
2	0	2	2	1	2	22 178.4592	0.0002	
3	0	3	3	1	3	22 178.4809	0.006	
3	1	3	3	0	3	22 178.5109	0.0049	
2	1	2	2	0	2	22 178.5326	0.0016	
1	1	1	1	0	1	22 178.5576	−0.0024	W1
2	2	1	2	1	1	22 178.6860	0.0010	W3
1	1	0	0	0	0	22 178.7861	−0.0009	W2
2	2	0	2	1	2	22 178.8261	−0.0009	
3	3	0	3	2	2	22 178.9240	−0.0020	
2	1	1	1	0	1	22 179.0096	−0.0044	
2	2	0	1	1	0	22 179.1096	−0.0014	
2	2	1	1	1	1	22 179.1363	−0.0007	W3
3	1	2	2	0	2	22 179.2656	0.0016	
3	2	1	2	1	1	22 179.3056	−0.0003	
3	2	2	2	1	2	22 179.3640	0.0020	
3	3	0	2	2	0	22 179.4607	−0.0013	
3	3	1	2	2	1	22 179.4691	−0.0039	
4	2	2	3	1	2	22 179.5191	−0.0059	
4	1	3	3	0	3	22 179.5358	−0.0022	
4	2	3	3	1	3	22 179.6058	0.0038	
4	3	1	3	2	1	22 179.6392	−0.0008	
4	3	2	3	2	2	22 179.6809	0.0019	
4	4	0	3	3	0	22 179.8077	−0.0053	

[a]Lines with the same labels (e.g., W1) have the same quantum beat patterns.

TABLE IV. Observed 0_0^0 E_2-E_1 transitions (cm^{-1}).

J'	Ka'	Kc'	J''	Ka''	Kc''	Obs.	Obs–cal.	Q.B.
1	1	1	2	2	1	22 177.9289	−0.002	W4
1	1	0	2	2	0	22 177.9585	−0.0005	W5
1	0	1	2	1	1	22 178.0590	−0.001	W6
0	0	0	1	1	0	22 178.2859	−0.001	
1	1	0	2	0	2	22 178.3258	0.003	
2	1	1	2	2	1	22 178.3793	−0.006	
1	0	1	1	1	1	22 178.5109	−0.001	W6
3	1	3	3	0	3	22 178.5843	0.002	
2	1	2	2	0	2	22 178.6060	−0.001	
1	1	1	1	0	1	22 178.6343	−0.003	W4
1	1	0	0	0	0	22 178.8628	−0.001	W5
2	1	1	1	0	1	22 179.0880	−0.002	
2	2	0	1	1	0	22 179.1880	0.003	
2	2	1	1	1	1	22 179.2089	−0.001	
3	1	2	2	0	2	22 179.3407	0.002	
3	2	1	2	1	1	22 179.3807	0.002	
3	2	2	2	1	2	22 179.4361	0.002	

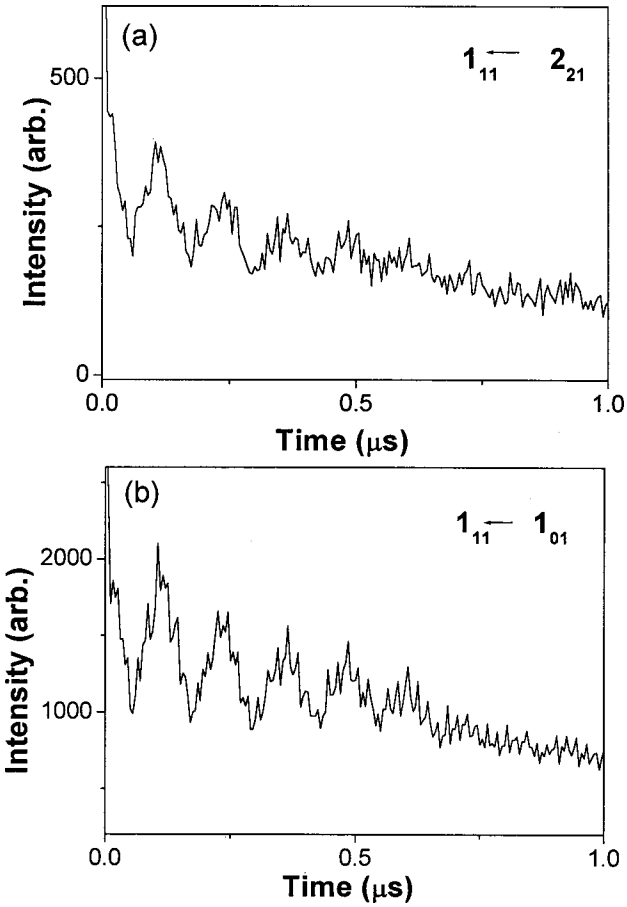

FIG. 3. Fluorescence quantum beat decay patterns of (a) $1_{11} \leftarrow 2_{21}$ and (b) $1_{11} \leftarrow 1_{01}$ transitions of the 0_0^0 band.

transitions from $J''=3$ and 4 observed at 3 atm stagnation pressure due to their low intensity.

B. 15_0^1 band

Transition to the first excited state of the gearing mode ν_{15} is not allowed in the C_{2h} point group, but it is allowed in the G_{36} permutation–inversion molecular symmetry group. The selection rules obtained from G_{36} show that two subbands are allowed, i.e., G–G and E_3-E_3. In agreement with this theoretical prediction, two subbands were observed in this region at 9 atm stagnation pressure, as shown in Fig. 4. The theoretical simulation[8] places the E_3-E_3 transition lower in frequency than the G–G transition. Therefore, we assigned the low-frequency band as the E_3-E_3 transition, and high-frequency band as the G–G transition.

The E_3-E_3 band can be described very well by the rigid rotor model. All of the observed transitions were assigned to c-type transitions with $\Delta K_a = odd$, $\Delta K_c = even$. Transitions of d-type with $\Delta K_a = even$, $\Delta K_c = even$, which are allowed by the selection rules, were not observed in this subband. The quantum beat decay patterns were also used in this band to confirm transition assignments. No other type of transition was observed in this band. The transition frequencies and assignments are listed in Table V.

The G–G transition frequencies cannot even be approximately described by the rigid rotor model. In the analysis of

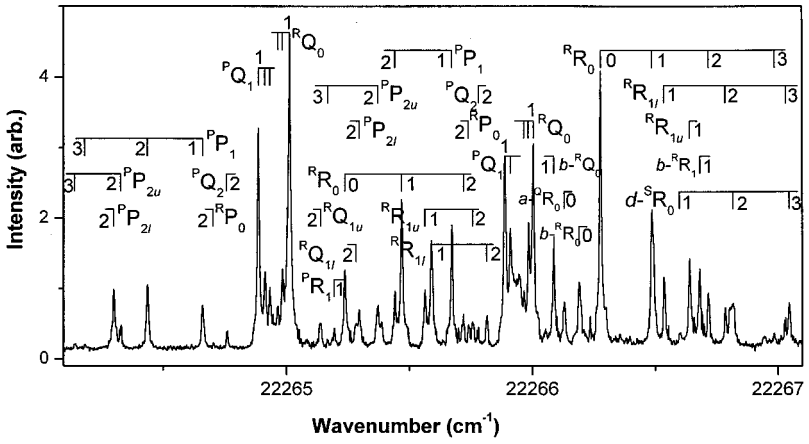

FIG. 4. Part of the spectrum of the 15_0^1 band.

this subband, ground state rotational constants obtained from the 0_0^0 band and the method of combination differences were thus used to make assignments. All transitions with the same upper state were confirmed by their quantum beat decay patterns. Some of the fluorescence decay patterns are shown in Fig. 5. It was found that in addition to $\Delta K_a = odd$, $\Delta K_c = even$ *c*-type transitions, *ab*-type transitions were observed, though their intensities are not as large as those for the *c*-type transitions. The *d*-type transitions, with $\Delta K_a = even$, $\Delta K_c = even$, which are allowed by the G_{36} selection rules (see Sec. III) were only partly observed, i.e., we did not observe any transitions with $\Delta K_a = 0$, $\Delta K_c = 0$. However, transitions with $\Delta K_a = 2$, $\Delta K_c = 0$ were observed, including the transitions $2_{21} \leftarrow 1_{01}$, $3_{22} \leftarrow 2_{02}$, and $4_{23} \leftarrow 3_{03}$. The assignments and transition frequencies are listed in Table VI. For the total of 57 lines we observed in this band, 54 lines are assigned.

TABLE V. Observed 15_0^1 $E_3 - E_3$ transitions (cm^{-1}).

J'	Ka'	Kc'	J''	Ka''	Kc''	Obs.	Obs−cal.	Q.B.
2	1	1	3	2	1	22 264.1495	0.0015	
2	0	2	3	1	2	22 264.1912	0.0018	
1	1	1	2	2	1	22 264.3053	0.0003	
1	1	0	2	2	0	22 264.3346	−0.0004	
1	0	1	2	1	1	22 264.4404	0.0004	V1
0	0	0	1	1	0	22 264.6605	−0.0015	
1	1	0	2	0	2	22 264.7082	0.0052	
2	1	1	2	2	1	22 264.7623	0.0003	V2
1	0	1	1	1	1	22 264.8874	0.0004	V1
2	0	2	2	1	2	22 264.914	0.0010	
3	0	3	3	1	3	22 264.9341	0.0031	
3	1	3	3	0	3	22 264.9674	0.0044	
2	1	2	2	0	2	22 264.9858	−0.0012	
1	1	1	1	0	1	22 265.0142	0.0002	
3	2	2	3	1	2	22 265.0884	−0.0096	
2	2	1	2	1	1	22 265.1433	0.0003	V3
2	0	2	1	1	0	22 265.1976	−0.0034	
1	1	0	0	0	0	22 265.2409	−0.0001	
2	2	0	2	1	2	22 265.2873	0.0083	
2	1	1	1	0	1	22 265.4711	0.0001	V2
2	2	0	1	1	0	22 265.5662	−0.0008	
2	2	1	1	1	1	22 265.5912	0.0012	V3
3	1	2	2	0	2	22 265.7229	−0.0011	
3	2	1	2	1	1	22 265.761	−0.0070	
3	2	2	2	1	2	22 265.8197	0.0017	

Only transition frequencies at 22 266.236, 22 266.811, and 22 266.948 cm^{-1} are not assigned.

C. 21_0^1 band

Four subbands are allowed in the 21_0^1 band. However, only three subbands are observed in this region, as shown in Fig. 6. Their vibronic assignments must be consistent with the types of rotational transitions they contain. These three subbands were assigned to $E_2 - E_1$, G–G, and $A_3 - A_1$ transitions, respectively, according to their rotational selection rules and the ordering of transition frequencies predicted by theory.[8]

The first subband, $E_2 - E_1$, at the lowest frequency, contains *ab*- and *cd*-type transitions. It was found that the transition frequencies of this subband could not be approximated by the rigid rotor model. Although most of the lines are assigned to *c*-type $\Delta K_a = odd$, $\Delta K_c = even$ transitions, *ab*-type transitions and *d*-type transitions were all observed. The intensities of *a*-, *b*-, and *d*-type transitions are about 0.2–0.5 times that of the *c*-type transition intensities. Most of the assignments were confirmed by the quantum beat decay patterns. Figure 7 shows quantum beat fluorescence decay patterns of four different transitions: $1_{11} \leftarrow 0_{00}$, $1_{11} \leftarrow 1_{01}$, 1_{11}

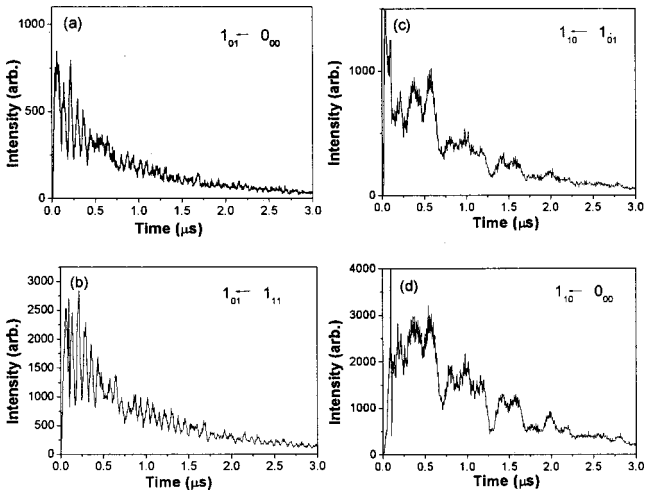

FIG. 5. Fluorescence quantum beat decay patterns of (a) $1_{01} \leftarrow 0_{00}$, (b) $1_{01} \leftarrow 1_{11}$, (c) $1_{10} \leftarrow 1_{01}$, (d) $1_{10} \leftarrow 0_{00}$ transitions of the 15_0^1 band.

TABLE VI. Observed 15_0^1 $G-G$ transitions (cm^{-1}).

J'	Ka'	Kc'	J''	Ka''	Kc''	Obs.	Q.B.
2	1	1	3	2	1	22 265.1707	Z1
1	1	1	2	2	1	22 265.2993	Z2
1	1	0	2	2	0	22 265.376	Z3
1	1	0	2	2	1	22 265.3894	Z3
1	0	1	2	1	1	22 265.4444	Z4
0	0	0	1	1	0	22 265.6746	
1	1	0	2	0	2	22 265.7438	Z3
2	1	1	2	2	1	22 265.7824	Z1
1	0	1	1	1	1	22 265.8877	Z4
2	0	2	2	1	2	22 265.911	
3	1	3	3	0	3	22 265.9644	
2	1	2	2	0	2	22 265.9844	
1	1	1	1	0	1	22 266.0027	Z2
3	2	2	3	1	2	22 266.0558	Z5
1	1	0	1	0	1	22 266.0895	Z3
1	0	1	0	0	0	22 266.1299	Z4
1	1	1	0	0	0	22 266.1923	Z2
1	1	0	0	0	0	22 266.2796	Z3
2	1	1	1	0	1	22 266.4881	Z1
2	2	1	1	1	1	22 266.5364	Z6
2	2	1	1	0	1	22 266.6037	Z6
2	2	0	1	1	0	22 266.6432	Z7
2	2	0	1	1	1	22 266.6849	Z7
3	1	2	2	0	2	22 266.7199	
3	2	2	2	1	2	22 266.7883	Z5
3	2	2	2	0	2	22 266.8205	
4	1	3	3	0	3	22 266.9858	
4	2	3	3	1	3	22 267.0319	Z8
4	2	3	3	0	3	22 267.0483	Z8

$\leftarrow 1_{11}$, $1_{11} \leftarrow 2_{11}$, belonging to *b*-, *c*-, *d*-, and *d*-type of transitions, respectively. They all have the same quantum beat fluorescence decay patterns because they all have the same upper state. The large intensities of *ab*-type transitions observed in this subband indicate a strong nuclear coordinate dependence of the dipole moment operator or electronic wave function in this subband.

The second subband, G–G, the largest intensity of these three subbands, and most of its lines were assigned to *c*-type $\Delta K_a = odd$, $\Delta K_c = even$ transitions. However, *ab* transitions with small intensities were also observed. On the other hand, *d*-type transitions with $\Delta K_a = even$, $\Delta K_c = even$ were not observed. Some of the transitions were confirmed by their

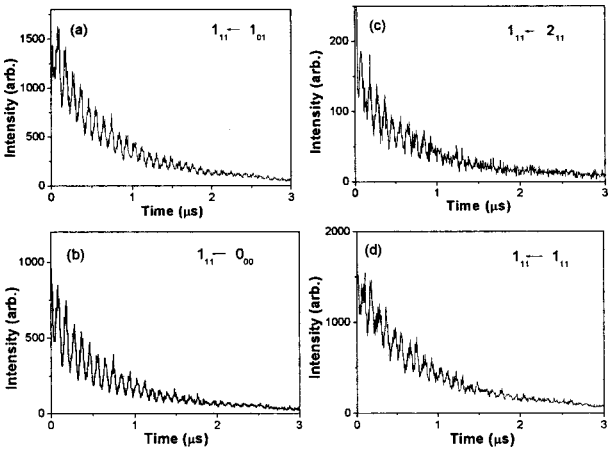

FIG. 7. Fluorescence quantum beat decay patterns of (a) $1_{11} \leftarrow 1_{01}$, (b) $1_{11} \leftarrow 0_{00}$, (c) $1_{11} \leftarrow 2_{11}$, (d) $1_{11} \leftarrow 1_{11}$ transitions of the 21_0^1 band.

fluorescence quantum beat decay patterns. It was found that the rigid rotor model does not fit this subband.

The third subband, A_3-A_1, has the smallest intensity and it contains only $\Delta K_a = even$, $\Delta K_c = odd$ transitions. Transitions with a rotational quantum number up to $J''=2$ were observed, and the positions were fit well by the rigid rotor model. It is interesting to note that the selection rules of *ab*-type vibronic transitions in an A_3-A_1 subband are $\Delta K_a = even$, $\Delta K_c = odd$ and $\Delta K_a = odd$, $\Delta K_c = odd$ transitions. However, only $\Delta K_a = even$, $\Delta K_c = odd$ transitions were observed.

For these three subbands, 68 lines were assigned. There are a total of about 10 lines lying in frequency between the E_2-E_1 and G–G subbands, and between the G–G and A_3-A_1 subbands which could not be assigned due to the low signal to noise ratio and the congested spectra in these regions. The observed frequencies and assignments for these three subbands are listed in Tables VII, VIII, and IX, respectively.

V. CONCLUSION

In summary, the difference between geometries of the methyl groups in the $X\,^1A_g$ and $A\,^1A_u$ states results in a long progression in the gearing and antigearing methyl torsions.

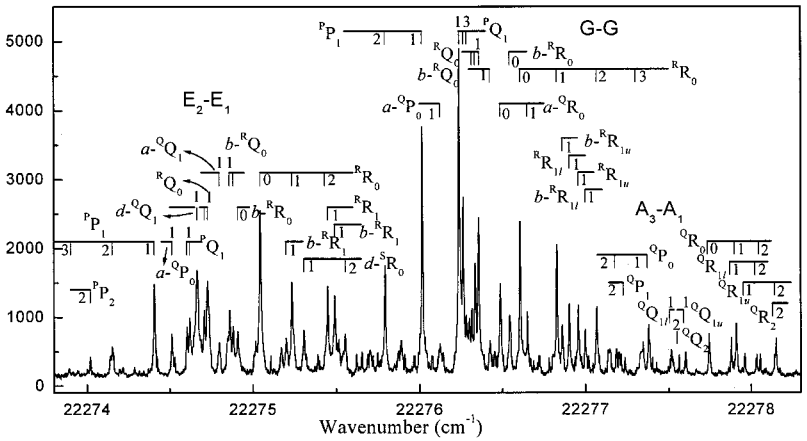

FIG. 6. Part of the spectrum of the 21_0^1 band.

TABLE VII. Observed 21_0^1 E_2-E_1 transitions (cm^{-1}). *: overlapped.

J'	Ka'	Kc'	J''	Ka''	Kc''	Obs.	Q.B.
2	1	2	3	2	2	22 273.801	X1
2	0	2	3	1	2	22 273.887	X2
2	1	1	3	2	1	22 273.914	X3
1	0	1	2	2	0	22 273.944	
1	1	1	2	2	0	22 274.004	X4
1	1	1	2	2	1	22 274.020	X4
1	1	0	2	2	0	22 274.140	
1	0	1	2	1	1	22 274.151	X5
1	1	1	2	1	1	22 274.210	X4
1	0	1	2	1	2	22 274.281	X5
0	0	0	1	1	0	22 274.402	
0	0	0	1	0	1	22 274.509	*
1	1	0	2	0	2	22 274.509	*
2	1	1	2	2	1	22 274.527	X3
1	0	1	1	1	1	22 274.601	X5
2	0	2	2	1	2	22 274.617	X2
1	1	1	1	1	1	22 274.662	X4
2	1	2	2	0	2	22 274.705	X1
1	1	1	1	0	1	22 274.726	X4
1	1	0	1	1	1	22 274.796	X6
1	0	1	0	0	0	22 274.842	X5
1	1	0	1	0	1	22 274.859	X6
2	1	1	2	0	2	22 274.879	X3
1	1	1	0	0	0	22 274.907	X4
1	1	0	0	0	0	22 275.041	X6
2	2	0	2	1	2	22 275.170	*
2	1	1	1	1	1	22 275.170	*
2	2	1	1	1	0	22 275.196	X7
2	1	1	1	0	1	22 275.231	
2	2	1	1	0	1	22 275.303	X7
2	2	0	1	1	0	22 275.446	X8
2	2	0	1	1	1	22 275.488	X8
			2	1	2	22 275.513	X9
			2	0	2	22 275.551	X9
			2	1	2	22 275.618	X10
			2	0	2	22 275.650	X10

TABLE VIII. Observed 21_0^1 $G-G$ transitions.

J'	Ka'	Kc'	J''	Ka''	Kc''	Obs.	Q.B.
1	0	1	2	1	1	22 275.791	Y1
0	0	0	1	1	0	22 276.015	Y2
1	1	0	2	1	2	22 276.043	Y3
0	0	0	1	0	1	22 276.124	Y2
1	0	1	1	1	1	22 276.239	Y1
1	1	1	1	1	0	22 276.263	Y4
3	0	3	3	1	3	22 276.283	
3	1	3	3	0	3	22 276.315	
2	1	2	2	0	2	22 276.335	
1	1	1	1	0	1	22 276.358	Y4
1	1	0	1	0	1	22 276.429	Y3
1	0	1	0	0	0	22 276.487	Y1
1	1	1	0	0	0	22 276.547	Y4
1	1	0	0	0	0	22 276.607	Y3
2	0	2	1	0	1	22 276.650	
2	1	1	1	1	0	22 276.722	Y5
2	1	1	1	0	1	22 276.827	Y5
2	2	1	1	1	0	22 276.860	Y6
2	2	1	1	1	1	22 276.902	Y6
2	2	0	1	1	0	22 276.955	Y7
2	2	0	1	1	1	22 276.997	Y7
3	1	2	2	0	2	22 277.067	

TABLE IX. Observed 21_0^1 A_3-A_1 transitions (cm^{-1}).

J'	Ka'	Kc'	J''	Ka''	Kc''	Obs.	Obs−cal.
1	1	1	2	1	2	22 277.224	−0.002
0	0	0	1	0	1	22 277.369	−0.001
1	1	1	1	1	0	22 277.504	−0.004
2	2	0	2	2	1	22 277.549	−0.005
1	1	0	1	1	1	22 277.589	−0.004
1	0	1	0	0	0	22 277.734	−0.001
2	1	2	1	1	1	22 277.869	−0.003
2	0	2	1	0	1	22 277.899	−0.001
2	1	1	1	1	0	22 277.951	−0.001
3	1	3	2	1	2	22 278.023	0.003
3	0	3	2	0	2	22 278.046	0.002
3	2	1	2	2	0	22 278.128	0.004
3	1	2	2	1	1	22 278.141	0.007

In this work, the laser-induced fluorescence of the first three torsional bands in the $A\ ^1A_u$ state were rotationally resolved. Because of the small rotational constants, it is possible to have rotationally resolved spectra only when the rotational temperature is below 2 K, and this is the first time that rotationally resolved spectra of biacetyl have been obtained and assigned.

Quantum beats were used to help make and to confirm assignments in the high-resolution spectrum. This turns out to be a very powerful tool for assigning congested spectra of large molecules. With this technique we could assign more than 90% of all measured lines of reasonable strength in the spectrum. Our analysis confirms the band origin of the $A\ ^1A_u-X\ ^1A_g$ transition suggested by Herschbach *et al.*[7] and predicted by Senent *et al.*[8] The rotational constants derived from the good asymmetric rotor fits do not change much with vibrational state for the levels studied in this work, except for the A constants in the A_3-A_1 subband. The difference of the A constant may result from the change of bond lengths and/or bond angles of the molecule, or from a difference in the internal rotation effects between different symmetry species. The rotational constants derived from this work are very different from the values obtained by Gurnick *et al.*[2] from their analysis of a lower-resolution spectra. However, they are close to the values estimated by Henke *et al.*[10] from the known covalent radii and 120° bond angles in the aldehyde groups.

A careful discussion of the differences in a C_{2h} point-group treatment and a G_{36} permutation-inversion group treatment for this molecule is presented. One of the most important results is the presence of $\Delta K_a=even$, $\Delta K_c=even$ transitions. Depending on the band, all four possibilities of ΔK_a, $\Delta K_c=ee$, *eo*, *oe*, and *oo* were observed with reasonable intensities in our spectra. Earlier theoretical tunneling splitting predictions for this two-top problem,[8] based on a quantum chemistry potential surface treatment, were found quite useful in the spectral analysis. In contrast, a rigid rotor asymmetric top treatment only works well for rotational levels of the first three low-energy subbands and the subband of A_3-A_1 symmetry. A full two-top treatment will be required for a quantitative analysis of all levels.

Future work from this laboratory will consist of assign-

ing vibronic bands higher in energy. Spectra are taken and are as good as the spectra in this work.

ACKNOWLEDGMENTS

The authors thank Dr. Jon Hougen for instruction and helpful discussion. The work was partly supported by the National Science Council of the Republic of China, under Contract No. NSC 90-2113-M-001-035.

[1] J. Chaiken, T. Benson, M. Gurnick, and J. D. McDonald, Chem. Phys. Lett. **61**, 195 (1979).
[2] J. Chaiken, T. Benson, M. Gurnick, and J. D. McDonald, J. Chem. Phys. **74**, 106 (1981).
[3] J. W. Sidman and D. S. McClure, J. Am. Chem. Soc. **77**, 6461 (1955).
[4] R. van der Werf and J. Kommandeur, Chem. Phys. **16**, 125 (1976).
[5] R. Campargue and B. Soep, Chem. Phys. Lett. **64**, 469 (1979).
[6] K. L. Saenger, J. D. Barnwell, and D. R. Herschbach, J. Phys. Chem. **86**, 216 (1982).
[7] M. L. Senent, D. C. Moule, Y. G. Smeyers, A. Toro-Labbe, and F. J. Penalver, J. Mol. Spectrosc. **164**, 66 (1994).
[8] Y. Chen, L. Pei, J. Jin, Y. Gao, X. Ma, and C. Chen, J. Chem. Phys. **111**, 6650 (1999).
[9] W. Henke, H. L. Selzle, T. R. Hays, S. H. Lin, and E. W. Schlag, Chem. Phys. Lett. **77**, 448 (1981).
[10] C. K. Ni and A. H. Kung, Opt. Lett. **21**, 1673 (1996).
[11] C. K. Ni and A. H. Kung, Appl. Opt. **37**, 530 (1998).
[12] (a) G. Herzberg, *Molecular Spectra and Molecular Structure, II. Infrared and Raman Spectra of Polyatomic Molecules* (Krieger, Malabar, FL, 1991); G. Herzberg, *Molecular Spectra and Molecular Structure, III. Electronic Spectra and Electronic Structure of Polyatomic Molecules* (Krieger, Malabar, FL, 1991).
[13] H. C. Longuet-Higgins, Mol. Phys. **6**, 445 (1963).
[14] P. R. Bunker and P. Jensen, *Molecular Symmetry and Spectroscopy* (NRC Research Press, Ottawa, 1998).
[15] D. D. Nelson, Jr. and W. Klemperer, J. Chem. Phys. **87**, 139 (1987).